

Cosmological Reionization Around the First Stars: Monte Carlo Radiative Transfer

B. Ciardi¹, A. Ferrara², S. Marri³ and G. Raimondo⁴

¹ *Università di Firenze, Largo Enrico Fermi 5, 50125 Firenze, Italy*

² *Osservatorio Astrofisico di Arcetri, Largo Enrico Fermi 5, 50125 Firenze, Italy*

³ *Max-Planck-Institut für Astrophysik, Karl-Schwarzschild-Straße 1, 85748 Garching, Germany*

⁴ *Osservatorio Astronomico di Collurania, Via Maggini, 64100 Teramo, Italy*

November 2000

ABSTRACT

We study the evolution of ionization fronts around the first proto-galaxies by using high resolution numerical cosmological (Λ +CDM model) simulations and Monte Carlo radiative transfer methods. We present the numerical scheme in detail and show the results of test runs from which we conclude that the scheme is both fast and accurate. As an example of interesting cosmological application, we study the reionization produced by a stellar source of total mass $M = 2 \times 10^8 M_\odot$ turning on at $z \approx 12$, located at a node of the cosmic web. The study includes a Spectral Energy Distribution of a zero-metallicity stellar population, and two Initial Mass Functions (Salpeter/Larson). The expansion of the I-front is followed as it breaks out from the galaxy and it is channeled by the filaments into the voids, assuming, in a 2D representation, a characteristic butterfly shape. The ionization evolution is very well tracked by our scheme, as realized by the correct treatment of the channeling and shadowing effects due to overdensities. We confirm previous claims that both the shape of the IMF and the ionizing power metallicity dependence are important to correctly determine the reionization of the universe.

Key words: galaxies: formation - intergalactic medium - cosmology: theory

1 INTRODUCTION

An increasing number of works has been recently dedicated to the study of the reionization of the universe (Gnedin & Ostriker 1997; Haiman & Loeb 1998; Valageas & Silk 1999; Ciardi *et al.* 2000, CFGJ; Miralda-Escudé, Haehnelt & Rees 2000; Chiu & Ostriker 2000; Bruscoli *et al.* 2000; Gnedin 2000; Benson *et al.* 2000) which use both analytical and numerical approaches. An important refinement has been introduced by the proper treatment of a number of feedback effects ranging from the mechanical energy injection to the H_2 photodissociating radiation produced by massive stars (CFGJ). However, probably the major ingredient still lacking for a physically complete description of the reionization process is the correct treatment of the transfer of ionizing photons from their production site into the intergalactic medium (IGM). Attempts based on different approximated techniques have been proposed (Razoumov & Scott 1999; Abel, Norman & Madau 1999; Norman, Paschos & Abel 1998; Gnedin 2000; Umemura, Nakamoto & Susa 1999), which sometimes are not readily implemented in cosmological simulations. Therefore, it is crucial to develop exact and fast methods that can eventually yield a better treat-

ment of the propagation of ionization fronts in the early universe. The first three papers are based on the ray-tracing method, whereas Gnedin (2000) uses the so called local optical depth approximation. Finally Umemura, Nakamoto & Susa (1999) implemented a time-independent ray-tracing method. Monte Carlo (MC) methods have been widely used in several physical/astrophysical areas to tackle radiative transfer problems (for a reference book see Cashwell & Everett 1959) and they have been shown to result in fast and accurate schemes. Here we build up on previous experience of our group (Bianchi, Ferrara & Giovanardi 1996; Ferrara *et al.* 1996; Ferrara *et al.* 1999; Bianchi *et al.* 2000) in dealing with MC problems to present a case study of cosmological H_{II} regions produced by the first stellar sources. The study is intended as a test of the applicability of the adopted techniques in conjunction with cosmological simulations in terms of convergence, accuracy, and speed of the scheme.

As an example of interesting cosmological application, we study the reionization produced by a stellar source of total mass $M = 2 \times 10^8 M_\odot$ turning on at $z \approx 12$, located at a node of the cosmic web. The study includes a Spectral Energy Distribution of a zero-metallicity stellar population,

and two Initial Mass Functions (Salpeter/Larson); the IGM spatial density distribution is deduced from high resolution cosmological simulations described below.

In a forthcoming paper we will then improve the results of CFGJ by exploiting the strength of the MC method to release the approximations relative to the radiative transfer made in that paper.

2 NUMERICAL SIMULATIONS

We have studied the evolution of small scale cosmic structure in a standard Λ +CDM model with $\Omega_\Lambda = 0.7$ and $\Omega_m = 0.3$. The baryon contribution to Ω_m is $\Omega_b = 0.04$, the adopted value of the Hubble constant is $H_0 = 70 \text{ km sec}^{-1} \text{ Mpc}^{-1}$.

The initial conditions are produced with the COSMICS^{*} code adopting a normalization $\sigma_8 = 1.14$ for the power spectrum. The initial particle distribution (at redshift $z = 103.2$) is made out of a 256^3 grid in a box of 4 Mpc (comoving), thus giving a mass per particle of about $1.5 \times 10^5 M_\odot$. We adopt vacuum boundary conditions; this requires the initial box to be reshaped. Assuming that tidal forces from large scale fluctuations are negligible for this problem, we cut a sphere of radius 2 Mpc from the initial cube and follow the evolution of the system in isolation. In practice, we study the evolution of a central sphere of radius about 1.2 Mpc in full mass resolution with a coarse re-sampling of the most external particles. In the hi-resolution (central) region the number of particles is 2313847, whereas the rebinning left us with 10008 particles of variable mass (increasing with distance from the center) in the external 1.2 – 2.0 Mpc shell.

We evolve this initial matter distribution with GADGET (Springel, Yoshida & White 2000), a parallel N-body tree-code with an SPH scheme to describe hydrodynamical processes. SPH particles are placed on top of hi-resolution dark matter particles with the same velocity and a low initial temperature (about 150 K, the temperature of intergalactic medium as determined by adiabatic expansion of the universe after decoupling); the mass of each fluid particle is rescaled according to the baryon and matter fraction quoted above. The (spline) softening length is 1 kpc for the gas particles, and 3 kpc for hi-resolution dark matter particles, respectively. For the problem at study here, the simulation is stopped at $z \approx 5$, thus avoiding the very strong nonlinear phase in which our assumption of zero tidal effects from large scale structure would break down.

The gas-dynamics evolution is purely adiabatic in order to reasonably limit the integration time. Thus, we are not able to follow the details of cooling processes that ultimately lead to the formation of very dense and cold star forming regions. However, the density field of the mildly overdense IGM should be reasonably well described by this assumption. Our mass resolution does not also allow a full resolution of the Jeans mass, and therefore the presence of sub-grid structure that we cannot track is expected. This is a problem common to all presently available simulations, implying that the treatment of IGM clumping is only approximate, as recently pointed out by Haiman, Abel & Madau (2000).

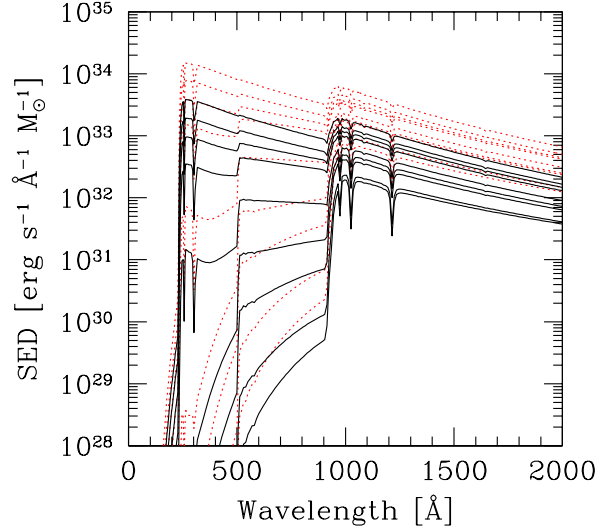


Figure 1. Evolution of the SED for a Simple Stellar Population of metal free stars for two different IMFs: Salpeter (solid lines) and Larson with $M_c = 5 M_\odot$ (dotted). The evolutionary times are, from the top to the bottom, 5, 7, 10, 15, 30, 50, 70, 100, 150 Myr.

Simulations were performed on the Cray-T3E at Rechenzentrum-Garching, the Joint Computing Center of the Max-Planck-Gesellschaft and Max-Planck-Institut fuer Plasmaphysik.

Finally, from the SPH particle temperature and density distribution we reconstruct a central cubic region of 128^3 cells, the grid values of any field being evaluated from particle values with an SPH-like interpolation. For the reionization study presented below, we have concentrated, as an example, on a source located at redshift $z \approx 12$ immersed in the density field calculated from the simulations described above. The location and mass of the dark matter halos in the simulation have been determined by means of a friend-of-friend algorithm. We have then selected a halo suitably located in the node of a cosmic filamentary structure and associated a luminous source to it. The total halo mass is $M = 2 \times 10^8 M_\odot$; the corresponding stellar mass has been determined following the same prescriptions of CFGJ, *i.e.*

$$M_\star = (\Omega_b/\Omega_m) M f_b f_\star, \quad (1)$$

where $f_b = 0.08$ is the fraction of virialized baryons able to cool and become available to form stars, and $f_\star = 0.15$ is the star formation efficiency. Although with our cell size of 15 kpc we are marginally able to resolve the source (comoving) virial radius (about 20 kpc), we do not attempt to treat the the escape of ionizing photons (Dove, Shull & Ferrara 2000; Wood & Loeb 2000) from the galaxy interstellar medium. Instead we take a fixed value for this quantity equal to $f_{esc} = 0.2$, the upper limit obtained by the above studies, by which we multiply the source ionizing photon flux.

^{*} Bertschinger, <http://arcturus.mit.edu/cosmics/>

3 POPIII STAR SPECTRUM AND IMF

The SEDs of metal free star systems used in this paper were calculated implementing the synthetic evolutionary code developed for a Simple Stellar Population (Brocato *et al.* 1999, Brocato *et al.* 2000). For a detailed description of the computational procedure we refer to those papers; here we just outline that the results of this code have been largely tested on young LMC clusters and old galactic globular clusters showing a very good agreement. The present synthesis models rely on the set of homogeneous evolutionary computations for stars with a cosmological amount of heavy elements and helium ($Z=10^{-10}$ and $Y=0.23$) presented by Cassisi & Castellani (1993) and Cassisi, Castellani & Tornambè (1996) and properly extended to higher masses in order to cover a wide range of ages. All the major evolutionary phases are taken into account, both the H and the He burning phase for stars with original masses in the range 0.7–40 M_{\odot} , for which the He burning phase is followed up to the Carbon ignition or, alternatively, to the onset of the thermal pulses. Models atmospheres are by Kurucz (1993) for metallicity $Z=2 \times 10^{-7}$. The available temperatures range from 3700 K to 50000 K, so the spectra at higher temperatures and gravity are simply extrapolated in order to keep the homogeneity of the grid. The wavelength range is from 91 Å to 160 μm and the spectral resolution is typically 10–20 Å in the UV to optical bands. We consider an instantaneous burst of star formation assuming that masses range from 1 M_{\odot} , as recently suggested for Pop III stars by Nakamura & Umemura (1999a, 1999b), to 40 M_{\odot} and two cases for the IMF: *i*) a standard Salpeter law, and *ii*) a Salpeter function at the upper mass end which falls off exponentially below a characteristic stellar mass M_c (Larson 1998). The last case is taken into account since both theory of thermo-dynamical condition of primordial gas and the absence of observations of solar mass, metal free stars seem to suggest at birth a paucity of low mass stars. Moreover, the mass interval used in this paper properly describes population models of age down to 5 Myr, the lifetime of a 40 M_{\odot} star; therefore, the burst models of this age are actually populated by 1–40 M_{\odot} stars. The resulting grid of SEDs were calculated at intervals of 1, 10 and 50 Myr between 1 and 20 Myr, 20 and 100 Myr, and 100 and 150 Myr, respectively. Other calculations of zero-metallicity star SEDs are present in the literature (see e.g. Cojazzi *et al.* 2000; Tumlinson & Shull 2000), but they do not show the detailed SED time evolution.

In Fig. 1 we show the adopted SEDs for the Salpeter IMF and the Larson IMF with $M_c = 5M_{\odot}$. The two sets of curves do not differ sensibly in their spectral shape evolution but the Larson IMF has about 4 times larger specific photon flux at the Lyman continuum. In Fig. 2 we show the time evolution of the total number of ionizing photons (in units of 10^{60}) emitted by a solar mass of metal free stars with the two IMFs. After about 10^7 yr both curves flatten as a consequence of the decreasing number of surviving massive stars. It is important to note that, during the first 5 Myr, a zero-metallicity stellar cluster with a Salpeter IMF has an ionizing photon rate about 25 times higher than the analogous one for a 1% solar metallicity used by CFGJ. As we will see later, this has important effects on the reionization process.

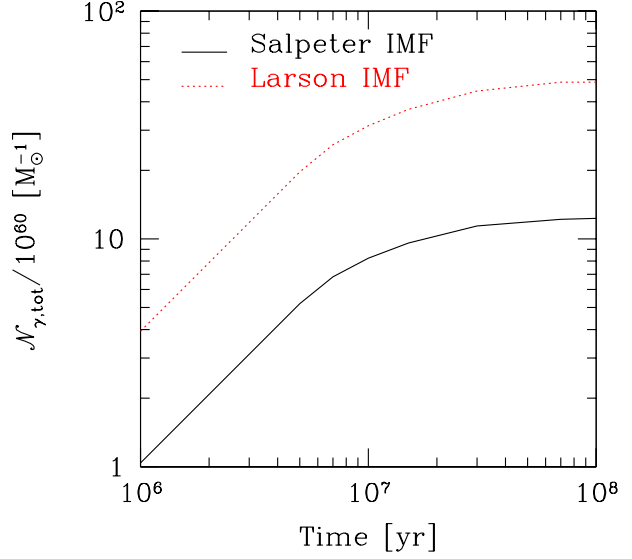


Figure 2. Time evolution of the total number of ionizing photons (in units of 10^{60}) emitted by a solar mass of metal free stars with a Salpeter (solid line) IMF and a Larson (dotted) IMF with $M_c = 5M_{\odot}$.

4 MONTE CARLO RADIATIVE TRANSFER

The application of MC schemes to radiative transfer problems requires that the radiation field is discretized in a representative number of photon packets, N_p . The processes involved (e.g. packet emission and absorption) are then treated statistically by randomly sampling the appropriate distribution function. Let us consider a source of bolometric luminosity L and lifetime t_s (L can be a function of time as our method easily allows to treat short-lived and variable sources). Packets have the same energy, \mathcal{E}_p , but contain a different number of monochromatic photons, N_{γ} , of frequency ν so that for the j -th packet it is $\mathcal{E}_p = N_{\gamma}(j)h\nu(j)$; their rate is $\dot{N}_p = L/\mathcal{E}_p$ and the simulation time when the j -th photon packet is emitted is then $t = jdt$ ($j = 1, \dots, N_p$), where $dt = \dot{N}_p^{-1}$. The number of photons in each packet emitted by the source during t_s is:

$$N_{\gamma}(j) = \frac{E_s}{N_p h \nu(j)} = \frac{L t_s}{N_p h \nu(j)}. \quad (2)$$

The packet frequency, ν , is obtained by sampling the source SED, $S(\nu)$: if R_{ν} is a random number, ν is given implicitly by:

$$R_{\nu} = \int_{\nu_H}^{\nu} d\nu' S(\nu') \left[\int_{\nu_H}^{\nu_{max}} d\nu' S(\nu') \right]^{-1}, \quad (3)$$

where ν_H is the threshold for hydrogen ionization.

We adopt spherical coordinates (r, θ, ϕ) with origin at the source location (x_s, y_s, z_s) in the box, such that the cartesian coordinates are:

$$\begin{aligned} x &= r \sin \theta \cos \phi & 0 \leq \phi \leq 2\pi, \\ y &= r \sin \theta \sin \phi & 0 \leq \theta \leq \pi, \\ z &= r \cos \theta. \end{aligned} \quad (4)$$

Assuming that the emission is isotropic and spherically symmetric, photon packets will propagate along the direction:

$$\hat{\mathbf{s}} \equiv [\hat{r}, \arccos(1 - 2R_\theta)\hat{\theta}, 2\pi R_\phi\hat{\phi}], \quad (5)$$

where R_θ and R_ϕ are random numbers. Note that the above choice automatically ensures a constant surface density of photon packets, thus preventing flux anisotropies at the poles due to angle sampling; this can be seen as follows. As we are sampling R_θ from a uniform distribution, the fraction of photon packets emitted in the angular range $\theta_1 < \theta < \theta_2$ is equal to

$$d\mathcal{N}_p(\theta_1, \theta_2) = (R_{\theta_2} - R_{\theta_1}), \quad (6)$$

where $R_{\theta_i} = (1/2)(1 - \cos \theta_i)$ from eq. 5. As the area fraction of the sphere belt delimited by θ_1 and θ_2 is

$$dA(\theta_1, \theta_2) = \frac{1}{2}(\cos \theta_1 - \cos \theta_2) \quad (7)$$

one sees that the surface density $d\mathcal{N}_p/dA$ of photon packets is constant and independent of angles.

Once emitted, a packet of frequency ν will travel for a finite path length of optical depth:

$$\tau_i(\nu) = \sigma(\nu) \sum_{k=1}^i (N_{\text{HI}})_k = \sigma(\nu) \sum_{k=1}^i (n_{\text{HI}})_k f \Delta x, \quad (8)$$

before being absorbed in the i -th grid cell. Here $\sigma(\nu)$ is the photoionization cross section, $(N_{\text{HI}})_k = (n_{\text{HI}})_k f \Delta x$ is the IGM neutral hydrogen column density through the k -th cell of size Δx ; the cell with $k = 0$ contains the source location and it is not included in the opacity count, as its contribution is already included in f_{esc} . For simplicity, the results presented here only include H opacity; inclusion of He, molecules (as H_2 and HD) and heavy elements, if present, is straightforward, although computationally expensive for molecules as one has to properly compute both the line widths and their Doppler shifts. The factor f accounts for the fact that the path through a cell is in the range $0 < \ell \leq \sqrt{3}\Delta x$ depending on its inclination. To limit the computational cost, we do not attempt to calculate the actual path and we treat this effect statistically as follows. Given a cubic box of unit size $\Delta x = 1$, via an independent Monte Carlo procedure, we randomly pick up on a face the coordinates of an entering ray and the direction of its propagation. We then derive the differential probability distribution function, $P(\ell)$, of the path lengths (Fig. 3) and define $f = 0.56$ as the median value of such distribution.

The value of i in eq. 8 is defined as the minimum one for which the following condition is satisfied:

$$\tau_i(\nu) \geq \tau = -\ln(1 - R_\tau), \quad (9)$$

with R_τ a random number. The previous relation is obtained by sampling the photon absorption probability distribution.

In each cell $k = 1, \dots, i$ along the path from the source to the absorption site of the j -th packet, we update the value of the hydrogen ionization fraction; $x = n_{\text{H}^+}/n_{\text{H}}$, n_{H^+} and n_{H} are the ionized and total hydrogen number density, respectively. This is done by advancing the time-dependent ionization equation in discretized form. At time $t = t^{n+1}$ it is:

$$x_k^{n+1} = x_k^n + \Delta t [\gamma_c(x_k^n) - \gamma_r(x_k^n)] + \frac{N_\gamma(j)}{(n_{\text{H}})_k(\Delta x)^3} \delta_{ki}; \quad (10)$$

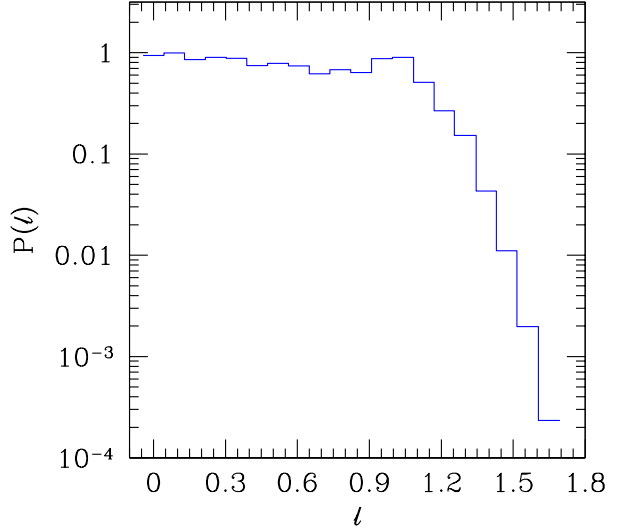


Figure 3. Differential probability distribution function of lengths, ℓ for randomly oriented paths entering from a face of a cubic box of unit size. The integral of the curve is normalized to unity.

γ_c and γ_r are the collisional ionization and recombination rates, respectively (Cen 1992); they are evaluated at the temperature of the gas in the cell. The initial temperature is increased to $T = 10^4$ K after absorption of a photon packet and set equal to $T = 2.734(1 + z)$, *i.e.* the CMB temperature, after the cell recombines (see below). This is a reasonable approximation, although T could be smaller at higher redshift (Ciardi, Ferrara & Abel 2000). The last term, describing photoionization due to photon packet absorption, is present only for the cell in which absorption takes place ($k = i, \delta_{ki} = 1$); in the other cells along the path ($k < i, \delta_{ki} = 0$) we simply follow the gas recombination. In case the derived value of $x_k^{n+1} > 1$, we set $x_k^{n+1} = 1$, and we use the extra photons to ionize the cell x_{k+1} . In practice, we write $N_\gamma(j) = N_\gamma^{(1)}(j) + N'_\gamma(j)$, where the number of photons required to obtain $x_k^{n+1} = 1$ is:

$$N_\gamma^{(1)}(j) = \{(1 - x_k^n) - \Delta t [\gamma_c(x_k^n) - \gamma_r(x_k^n)]\} (n_{\text{H}})_k (\Delta x)^3. \quad (11)$$

The most delicate point of the ionization fraction evaluation is to find an appropriate expression for Δt . In principle, one could update the ionization state on the entire grid after each photon packet emission. However, this is computationally too expensive. For this reason we choose to update the ionization state of cells along the packet path and we deduce Δt as follows.

The cell in which the source is located is enclosed by a cubic surface (shell). If we define the *order* of this shell to be $g = 1$, the number of its member cells is given by:

$$N_s(g) = (2g + 1)^3 - (2g - 1)^3 = 2(12g^2 + 1) \quad g \geq 1, \quad (12)$$

or $N_s(1) = 26$. The second order shell ($g = 2$) is instead made of 98 cells and so on. As the photon packet directions are isotropically distributed, statistically a cell in a shell of order g will be along a path every $[N_s(g)]^{-1}$ packets. Therefore the typical time scale between two subsequent ionization

fraction updates is $\Delta t = N_s(g)dt$; this is the value we use in eq. 10 above. The order g is calculated as:

$$g = \text{Max}[k_x, k_y, k_z], \quad (13)$$

where the k_i 's indicate the discrete cartesian coordinates of the cell in the reference frame eq. 4. The above approximation sets a lower limit on \mathcal{N}_p , as in order to be valid it is necessary that the update time Δt is shorter than the average recombination time, $\langle t_r \rangle$, in the box. Hence to advance the simulation up to a time t_s the number of packets required is:

$$\mathcal{N}_p \gtrsim 24N^2 \frac{t_s}{\langle t_r \rangle}, \quad (14)$$

where N^3 is the total number of cells in the box. This detailed treatment of recombination is important to accurately evaluate the optical depth through eq. 8.

We then introduce an ionization vector (size N^3) whose elements are initially set to zero. The vector element corresponding to a cell for which the ionization fraction is increased above $x_{th} = 0.99$ as a result of an absorption event is updated to contain the value:

$$j_r = \text{Int} \left[\frac{t_r(x_k, n_k) + t}{dt} \right], \quad (15)$$

where $t_r(x_k, n_k)$ is the local recombination time and t is the current simulation time. If further absorption does not take place before the time $j_r dt$, we allow for recombination emission from the given cell; if instead another absorption event takes place, we re-update the vector element to a new value of j_r . As already mentioned, after recombination, the cell temperature is set at the CMB temperature at that redshift.

Following a cell recombination a packet is emitted along a random direction from the same location. The probability that the emitted packet has $h\nu(j) > 13.6$ eV is given by the ratio between the number of recombinations to the ground level and the total one, *i.e.* 50% for $T = 10^4$ K. The frequency of the re-emitted packet is determined through eq. 3, where the source SED is substituted by the volume emissivity of the diffuse radiation, given by the Milne relation:

$$S_d(\nu) = \frac{2h\nu^3}{c^2} \frac{g_i}{g_{i+1}} \left(\frac{h^2}{2\pi n_p k T_e} \right)^{3/2} \times \sigma(\nu) e^{-h(\nu - \nu_H)/(kT_e)} n_{H+n_e}, \quad (16)$$

where g_i and g_{i+1} are the hydrogen ground level statistical weights; T_e and n_e are the electron temperature and number density. The propagation and absorption of re-emitted packets is then followed in the same manner as for primary ones. The only difference is that the opacity contribution of the re-emitting cell is now included.

The method is easily generalized to include an arbitrary number of point sources once the packet emission rates, and hence their emission sequence for the various sources are given.

4.1 Testing the Method

The method described in the previous Section has been tested against the analytical solution for the temporal evo-

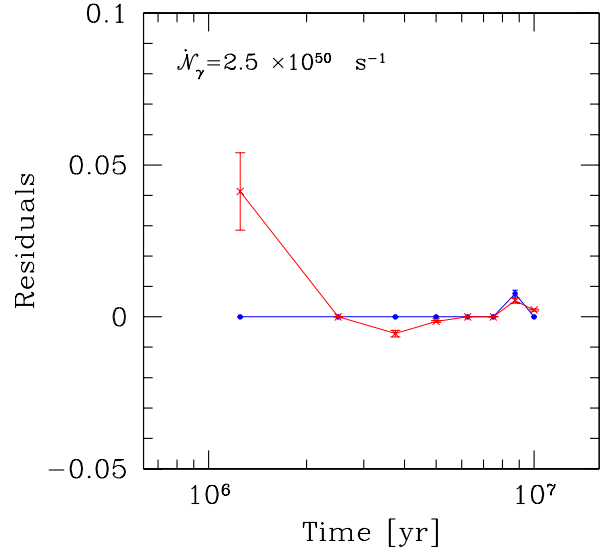


Figure 4. Residuals of the numerical HII region equivalent radius, R_n , for the convergency test: crosses refer to D^5 , circles to D^{50} (see text for definition of D). The source has ionizing photon rate $\dot{\mathcal{N}}_\gamma = 2.5 \times 10^{50} \text{ s}^{-1}$.

lution of the radius of an HII region produced by a source with constant ionizing rate and expanding in an homogeneous medium (Donhaue & Shull 1987; Shapiro & Giroux 1987). The HII region equivalent radius, R_n , is numerically derived by first assuming that a cell k is in the ionized state when $x_k > x_{th} = 0.99$. If N_{ion} is the number of ionized cells in the box, the volume occupied by the ionized region is $V = \Delta x^3 N_{ion}$ and the equivalent radius is then $R_n = (3V/4\pi)^{1/3}$. In all the tests presented here the gas density is set equal to average IGM one in an Einstein-de Sitter universe with $\Omega_b h^2 = 0.019$ at $z = 11.6$, *i.e.* $n_H = 4.5 \times 10^{-4} \text{ cm}^{-3}$; the adopted spectrum is monochromatic, with a photon energy equal to 13.6 eV.

First, we check for convergency of our scheme. We run three simulations with different values of $\mathcal{N}_p = (5, 50, 500) \times 10^5$. The source ionizing photon rate is $\dot{\mathcal{N}}_\gamma = 2.5 \times 10^{50} \text{ s}^{-1}$. For each run we calculate the residuals with respect to the highest resolution run $\mathcal{N}_p = 500 \times 10^5$; they are defined as:

$$D^y = \frac{R_n^y - R_n^{500}}{R_n^{500}}, \quad (17)$$

where the superscript $y = 5, 50$ refers to the low- and medium-resolution runs, respectively. The residuals are shown in Fig. 4 at different evolutionary times together with the associated mean quadratic errors; the error on R_n is assumed to be equal to Δx . Satisfactory convergency is achieved by the medium-res run; subsequent tests have hence been done using $\mathcal{N}_p = 50 \times 10^5$. For reference, this run takes only $\simeq 300$ s (CPU time) on a SUN ULTRA10/333MHz workstation.

Next, we assess the accuracy of the solution. In Fig. 5a we show the time evolution of R_n , as produced by sources of different ionizing photon rates $\dot{\mathcal{N}}_\gamma = (2.5, 12.5, 25, 125) \times 10^{50} \text{ s}^{-1}$, compared to the corresponding analytical radius, R_a . Fig. 5b shows the residuals (defined analogously to

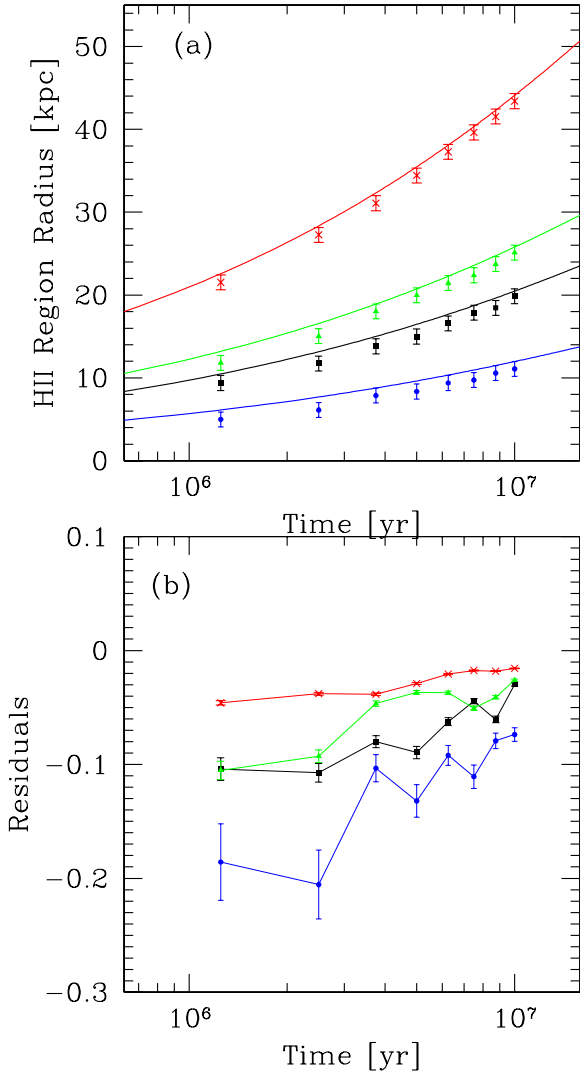


Figure 5. (a) Time evolution of the equivalent HII radius produced by sources of different ionizing photon rate $\dot{N}_\gamma = 2.5$ (circles), 12.5(squares), 25(triangles), 125(crosses) $\times 10^{50} \text{ s}^{-1}$, compared to the analytical solutions (solid lines). (b) Residuals of the numerical radii calculated with respect to the analytical ones. The notation is the same as in Fig. (a).

eq. 17 with R_n^{500} substituted by R_a) with respect to the analytical solution. In the worst case (very faint source, early evolutionary times) the residual is about 20%; This relatively large discrepancy occurs because the size of the ionized region is only a few cells. At later times and/or for more luminous sources the agreement is remarkably good, *i.e.* within a few percent.

Finally, we check the effects of varying the spatial resolution. To this aim we have considered runs with different box sizes, keeping a fixed linear number of cells $N = 128$. In Fig. 6 we show the residuals for runs with a box size $(1, 0.2, 0.1) \times N\Delta x$ with respect to the highest spatial resolution run for a source ionizing photon rate $\dot{N}_\gamma = 2.5 \times 10^{50} \text{ s}^{-1}$.

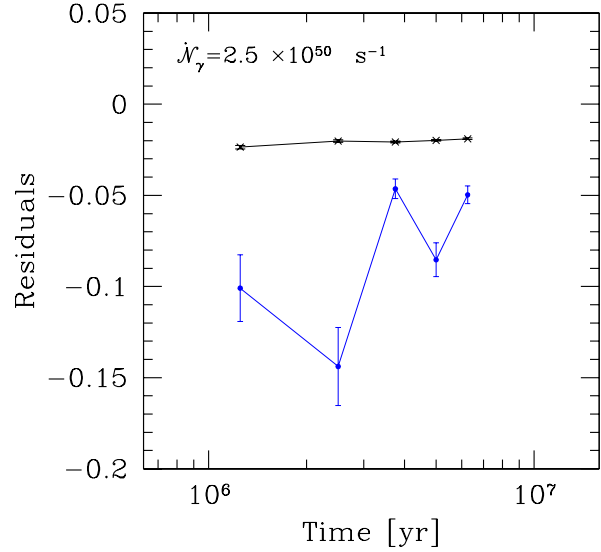


Figure 6. Residuals for runs with a comoving box size $(1, 0.2) \times N\Delta x$ (circles and crosses, respectively) with respect to one with $N\Delta x/10$. The source ionizing photon rate is $\dot{N}_\gamma = 2.5 \times 10^{50} \text{ s}^{-1}$.

5 RESULTS AND DISCUSSION

The combined cosmological and radiative transfer simulations described above allow us to determine the evolution of the ionized region around the selected zero-metallicity stellar object. Illustrative slices extracted from our simulation box through the source location are shown in Fig. 7 at different times (10, 20, 40, 60, 100 Myr) after the source has been turned on and a for Larson IMF, together with the initial density field. The above time interval corresponds to less than two redshift units at $z \approx 12$, and it is therefore not unreasonable for the purposes of this paper to neglect the IGM density evolution. As seen from Fig. 7, the ionization front (I-front) breaks out from the galaxy very rapidly, leaving behind a very clumpy ionization structure in the immediate surroundings where the IGM is overdense and, consequently, recombination times are shorter. As an aside, it is interesting to note that, as the circular velocity of the parent galaxy is a few km s^{-1} , the ionized gas (whose sound speed is of order of 10 km s^{-1}) will very likely be able to leave the galaxy, thus quenching further star formation. If this is a widespread phenomenon, it might have strong implications for the evolution of dwarf galaxies as already outlined by some authors (Barkana & Loeb 1999; Ferrara & Tolstoy 2000). Once the I-front expands in the IGM, it is channelled – for similar reasons – by the large filaments into the underdense volumes (voids) and its structure becomes very complex and jagged, assuming, in a 2D representation, a characteristic butterfly shape. The typical overdensity of the clumps encountered by the expanding I-front is ≈ 30 . Qualitatively, the typical final extent of the ionized region is of about 1 comoving Mpc; this size is reached already after 60 Myr. After that time, the rapid decrease of the source ionization power (Fig. 2) slows down the expansion. The final stage of the evolution is constituted by a relic HII region which slowly starts to recombine on a time scale which in the voids can be as

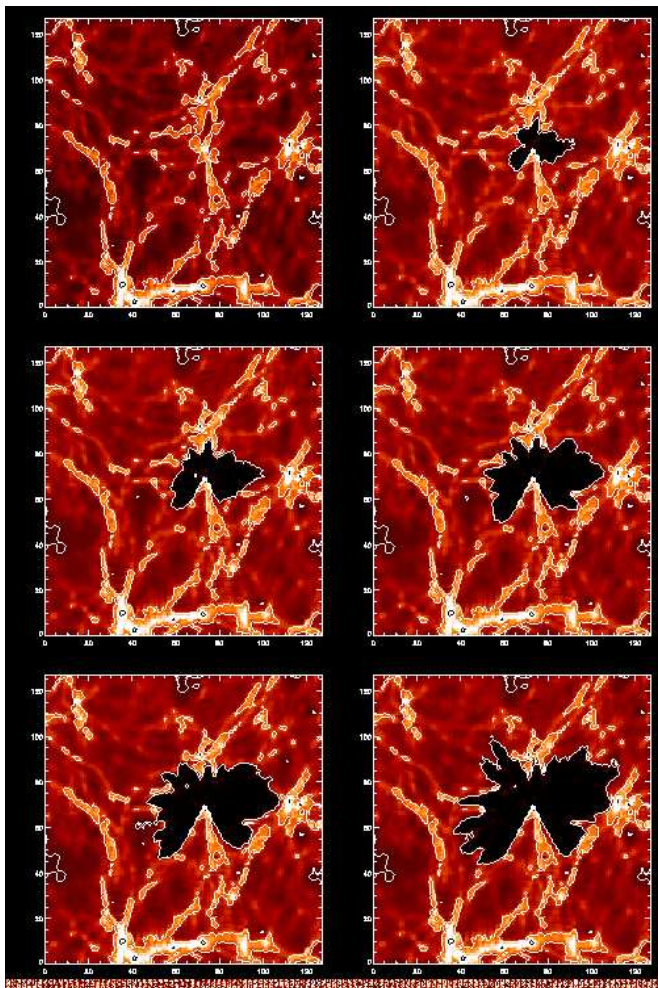


Figure 7. Slices through the simulation box containing a metal free stellar source of total mass $M = 2 \times 10^8 M_\odot$ at $z \approx 12$ in a Λ +CDM cosmological density field and a Larson IMF. The six panels show the neutral hydrogen number density, superposed to which (black regions) is the evolution of the ionized ($x > x_{th} = 0.99$) hydrogen distribution at times 0, 10, 20, 40, 60, and 100 Myr after source turn on. The linear (proper) size of each slice is 160 kpc.

long as 0.8 Gyr. The MC technique shows here all his power in following the details of the I-front evolution. For example, it tracks remarkably well the channeling induced by the large scale structure: the ionization front cannot propagate inside the densest filaments due to their large optical depth and short recombination time. In addition, also the effects of shadowing produced by isolated clumps are clearly recognized from the fingers protruding from the H_{II} region to the left of the source in the upper panel of Fig. 8. The ionization cone visible below the source, caused by a large overdensity located close to the source in that direction, is also a result of shadowing. Thus it seems that our scheme is highly suitable at least for this type of cosmological radiative transfer calculations.

We now turn to the differences induced by our two assumptions concerning the IMF. Fig. 8 shows a comparison between the final stages (100 Myr after the source turn on) of the I-front evolution for a Larson (upper panel) and a

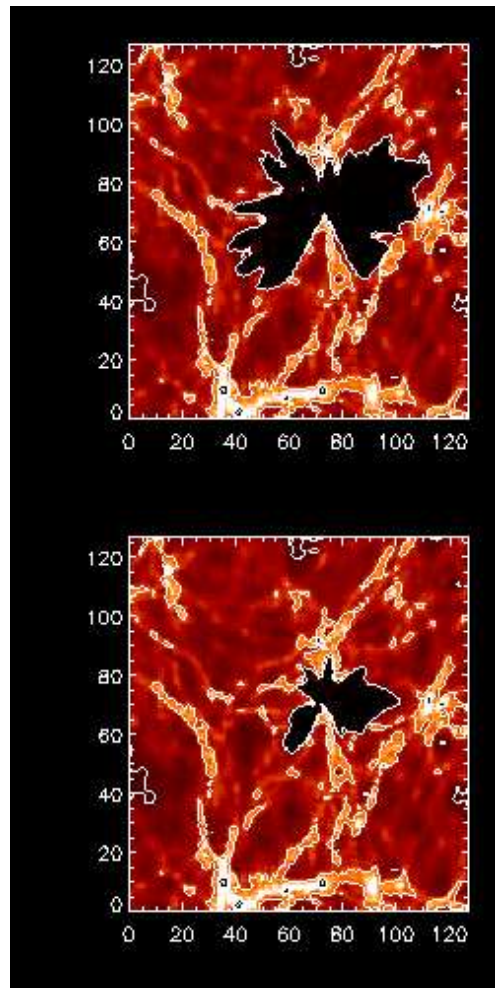


Figure 8. Comparison between the final stages ($t = 100$ Myr) of the I-front evolution for a Larson (upper panel) and a Salpeter (bottom) IMF for the same source properties as in Fig. 7.

Salpeter (bottom) IMF. The source stellar mass and other properties of the simulations are the same as those discussed above. For a Salpeter IMF, the volume of the ionized region is smaller by a factor 8, although the shape is very similar to the one for a Larson IMF case at an earlier stage, roughly corresponding to 10 Myr (see Fig. 7). This was expected from the two adopted SEDs. In fact, the total number of ionizing photons (see Fig. 2) per stellar mass formed integrated over the entire source lifetime and spectral extent is 5×10^{61} (10^{61}) for the Larson (Salpeter) IMF. Thus, the IMF might play an important role for the reionization of the universe; in addition, zero-metallicity stars have larger ionizing power as already stressed previously and recently addressed by other authors (Cojazzi *et al.* 2000; Tumlinson & Shull 2000).

To assess the differences between the evolution of an I-front propagating in an inhomogeneous medium, as in the simulations discussed here, and in a homogeneous gas at the mean IGM density, we have calculated the ratio $\mathcal{V} = V/V_h$ between the ionized volumes in our simulation and in the homogeneous case. This is found to be roughly independent of time and equal to $\mathcal{V} = 0.45$ for the Larson IMF. In the Salpeter IMF case \mathcal{V} varies slightly with time

from 0.125 to 0.2. Hence, this result confirms that the ionized volume tends to be smaller in the inhomogeneous case, but suggests that the effect is not dramatic.

ACKNOWLEDGMENTS

We would like to thank S. Cassisi for providing us with the stellar tracks; N. Yoshida and V. Springel for advises in various numerical problems; the referee T. Abel for useful comments. This research was supported in part by the National Science Foundation under Grant No. PHY94-07194 (SM) and by the Italian Ministry of University, Scientific Research and Technology (MURST) (GR).

REFERENCES

- Abel, T., Norman, M. L. & Madau, P. 1999, *ApJ*, 523, 66
 Barkana, R. & Loeb, A. 1999, *ApJ*, 523, 54
 Benson, A. J., Nusser, A., Sugiyama, S. & Lacey, C. G. 2000, preprint (astro-ph/0002457)
 Bianchi, S., Ferrara, A. & Giovanardi, C. 1996, *ApJ*, 465, 127
 Bianchi, S., Ferrara, A., Davies, J. & Alton, P. 2000, *MNRAS*, 311, 601
 Brocato, E., Castellani, V., Raimondo, G. & Romaniello, M. 1999, *A&AS*, 136, 65
 Brocato, E., Castellani, V., Poli F. M. & Raimondo, G. 2000, *A&A*, submitted
 Bruscoli, M., Ferrara, A., Fabbri, R. & Ciardi, B. 2000, *MNRAS*, 318, 1068
 Cashwell, E.D. & Everett, C.J. 1959, *A Practical Manual on the Monte Carlo Method for Random Walk Problems* (New York: Pergamon)
 Cassisi, S. & Castellani, V. 1993, *ApJSS* 88, 509
 Cassisi, S., Castellani, V. & Tornambè A. 1996, *A&A*, 317, 108
 Cen, R. 1992, *ApJS*, 78, 341
 Chiu, W. A. & Ostriker, J. P. 2000, preprint (astro-ph/9907220)
 Ciardi, B., Ferrara, A. & Abel, T. 2000, *ApJ*, 533, 594
 Ciardi, B., Ferrara, A., Governato, F. & Jenkins, A. 2000, *MNRAS*, 314, 611, CFGJ
 Cojazzi, P., Bressan, P., Lucchin, F., Pantano, O. & Chavez, M. 2000, *MNRAS*, 315, 51
 Donahue, M. & Shull, M. J. 1987, *ApJ*, 232, L13
 Dove, J. B. , Shull, J. M. & Ferrara, A. 2000, *ApJ*, 531, 846
 Ferrara, A., Bianchi, S., Dettmar, R.-J. & Giovanardi, C. 1996, *ApJL*, 467, 69
 Ferrara, A., Bianchi, S. Cimatti, A. & Giovanardi C. 1999, *ApJSS*, 123, 437
 Ferrara, A. & Tolstoy, E. 2000, *MNRAS*, 313, 291
 Gnedin, N. Y. 2000, preprint (astro-ph/0002151)
 Gnedin, N. Y. & Ostriker, J. P. 1997, *ApJ*, 486, 581
 Haiman, Z. & Loeb, A. 1998, *ApJ*, 503, 505
 Haiman, Z., Abel, T. & Madau, P. 2000, preprint (astro-ph/0009125)
 Kurucz, R. L. 1993, CDRom n. 13
 Larson, R. B. 1998, *MNRAS* 301, 569
 Miralda-Escudé, J., Haehnelt, M. & Rees, M. R. 2000, *ApJ*, 530, 1
 Nakamura, F. & Umemura, M., 1999a, *A&A*, 343, 41
 Nakamura, F. & Umemura, M., in *Star Formation 1999b*, Proc. of Star Formation 1999, held in Nagoya, Japan, Ed. T. Nakamoto, Nobeyama Radio Observatory, p. 28-29
 Norman, M. L., Paschos, P. & Abel, T. 1998, in *H₂ in the Early Universe*, Florence, Proc., eds. E. Corbelli, D. Galli & F. Palla, p. 455.
 Razoumov, A. & Scott, D. 1999, *MNRAS*, 309, 287
 Shapiro, P. R. & Giroux, M. L. 1987, *ApJ*, 321, L107
 Springel, V., Yoshida, N. & White, S. D. M. 2000, preprint (astro-ph/0003162)
 Tumlinson, J. & Shull, J. M. 2000, *ApJ*, 528, 65
 Umemura, M., Nakamoto, T. & Susa, H. 1999, in *Numerical Astrophysics*, eds. Miyama *et al.* (Kluwer: Dordrecht), p.43
 Valageas, P. & Silk, J. 1999, *A&A*, 347, 1
 Wood, K. & Loeb, A. 2000, *ApJ*, in press